Developmental Biology 419 (2016) 19–25

Contents lists available at ScienceDirect

Developmental Biology

journal homepage: www.elsevier.com/locate/developmentalbiology

Multi-sample Arabidopsis Growth and Imaging Chamber (MAGIC) for long term imaging in the ZEISS Lightsheet Z.1

Maria Angels de Luis Balaguer [a,1], Marina Ramos-Pezzotti [a,1], Morjan B. Rahhal [a,b], Charles E. Melvin [a,c,e], Eva Johannes [d], Timothy J. Horn [e,*], Rosangela Sozzani [a,*]

[a] Plant and Microbial Biology Department, North Carolina State University, Raleigh, USA
[b] Biological Engineering Department, North Carolina State University, Raleigh, USA
[c] Physics and Biology Departments, North Carolina State University, Raleigh, USA
[d] Cellular and Molecular Imaging Facility, North Carolina State University, Raleigh, USA
[e] Industrial and Systems Engineering Department, North Carolina State University, Raleigh, USA

ARTICLE INFO

Article history:
Received 24 February 2016
Received in revised form
28 April 2016
Accepted 24 May 2016
Available online 26 May 2016

Keywords:
Arabidopsis root
Light sheet
3D printing
Time-lapse imaging

ABSTRACT

Time-course imaging experiments on live organisms are critical for understanding the dynamics of growth and development. Light-sheet microscopy has advanced the field of long-term imaging of live specimens by significantly reducing photo-toxicity and allowing fast acquisition of three-dimensional data over time. However, current light-sheet technology does not allow the imaging of multiple plant specimens in parallel. To achieve higher throughput, we have developed a Multi-sample *Arabidopsis* Growth and Imaging Chamber (MAGIC) that provides near-physiological imaging conditions and allows high-throughput time-course imaging experiments in the ZEISS Lightsheet Z.1. Here, we illustrate MAGIC's imaging capabilities by following cell divisions, as an indicator of plant growth and development, over prolonged time periods. To automatically quantify the number of cell divisions in long-term experiments, we present a FIJI-based image processing pipeline. We demonstrate that plants imaged with our chamber undergo cell divisions for >16 times longer than those with the glass capillary system supplied by the ZEISS Z1.

1. Introduction

Understanding the dynamics underlying plant growth requires quantitative analyses of the organism's development over time. A key strategy to perform quantitative analyses of plant development over time is the observation of spatiotemporal cues in *in vivo* specimens (Reynaud et al., 2008). Confocal laser scanning microscopy, spinning disk microscopy, and epifluorescence platforms have been typically used to study such developmental cues through the visualization of fluorescently tagged proteins, individual cells, and tissue types at specific developmental stages (Ovečka, 2015). However, photo-induced cellular toxicity and fluorophore bleaching impose severe time limitations on the use of these microscopy tools (Sena et al., 2011). Consequently, the use of these tools is generally limited to imaging developmental processes that occur in short time-span intervals of seconds to minutes (von Wangenheim et al., 2014), although microfluidics devices have been developed that have allowed longer imaging experiments (Grossmann, 2011; Busch, 2012).

A technical advance has been achieved with the use of light sheet fluorescence microscopy (LSFM). In LSFM, the sheet of light that illuminates the specimen is orthogonal to the detection path (Maizel et al., 2011) and only fluorophores close to the focal plane of the detection system contribute to potential phototoxicity (Reynaud et al., 2008). By reducing photobleaching effects while imaging, the specimen is exposed to 5000 times less energy than in a confocal microscope (von Wangenheim et al., 2014). Furthermore, the light sheet has a unique stage set up that is well suited for imaging plant organisms. The specimen is suspended vertically, which allows for roots to follow the gravity vector. The light sheet stage allows for 3-dimensional movement and rotation around a vertical axis, such that imaging from all angles is possible (Reynaud et al., 2008). Additionally, data acquisition in LSFM technology allows the detector to collect all pixels in one image as opposed to one pixel at a time, which has a great impact on the rate of image acquisition –100 frames per second, in contrast to the confocal at 1–5 frames per second (Reynaud et al., 2008;

* Corresponding authors.
E-mail addresses: tjhorn.ims@gmail.com (T.J. Horn), ross_sozzani@ncsu.edu (R. Sozzani).
[1] These authors contributed equally to this work.

http://dx.doi.org/10.1016/j.ydbio.2016.05.029
0012-1606/

Weber and Huisken, 2011). As a result, LSFM permits lengthier imaging time course experiments than conventional microscopes and possesses unique characteristics well-suited for imaging plants. Accordingly, LSFM has been used to study longer developmental events such as plant organogenesis and lateral root formation (Sena et al., 2011; Maizel et al., 2011; Vermeer, 2014 Vermeer and Geldner, 2015).

Although LSFM overcomes multiple long-term imaging issues, certain challenges remain when imaging plants. First, only one specimen can be imaged at a time, preventing the imaging process from scaling up. This becomes a limiting factor for long-term experiments, where obtaining biological replicates significantly increases time and economic costs. Second, the specimen to be imaged needs to be transferred and loaded from its original growing plate into an imaging capillary system, which can be time-consuming and can generate a stress response in the plant. Moreover, when loaded in the capillary system provided by ZEISS for imaging, both shoot and root are embedded in agar. This prevents the shoot from exchanging gases, thereby inducing an extreme, rapid stress response in the plant. Although previous protocols have addressed the drawback of transferring plants to a glass capillary or having the shoot embedded in agar (Ovečka, 2015; Sena et al., 2011; von Wangenheim et al., 2014; Maizel et al., 2011; Novák et al., 2015), no attempt has been made to scale-up the number of plants imaged in the same experiment.

To address these issues, we designed a growth chamber and imaging device compatible with the ZEISS Lightsheet Z.1. This 3D printed device, the Multi-sample *Arabidopsis* Growth and Imaging Chamber (MAGIC), currently allows us to grow and image 4 *Arabidopsis* roots during the same experiment, eliminating the need to transfer samples while scaling up the imaging process. Moreover, MAGIC allows the shoots to grow outside of the agar, allowing gas exchange during the imaging process. We developed a protocol for planting, growing, and imaging *Arabidopsis* plants in MAGIC. We describe a semi-automatic image processing pipeline to perform the analysis of the acquired data. Using this imaging protocol, we validated MAGIC's imaging capabilities. We showed that roots that were imaged with MAGIC undergo significantly lower levels of stress than those imaged with the ZEISS glass capillary imaging system, resulting in considerable improvements in plant development and growth in each long-term imaging session.

2. Results

2.1. MAGIC allows growth and imaging of multiple roots

We designed MAGIC as a device where multiple plants are imaged in near physiological conditions (Fig. 1). Our 3D printed device takes advantage of the ZEISS stage setup, which allows the

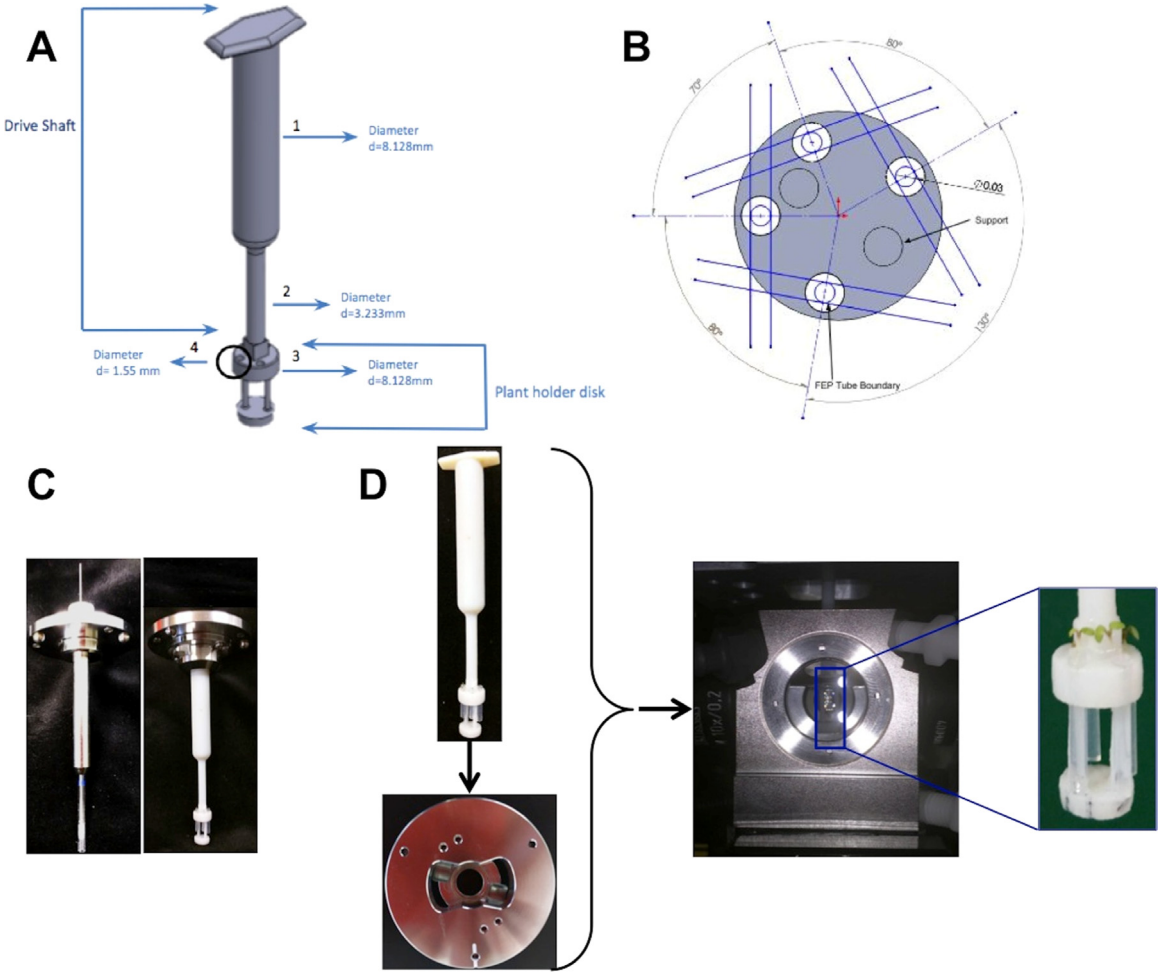

Fig. 1. A. 3D-Computer-Aided Design (CAD) model of MAGIC. Parts and dimensions are labeled in blue. B. Cross-sectional bottom view of the plant holder disk. The two blue lines around each sample indicate the range of motion of the light sheet when doing a z-stack. Holes are positioned in such a way that neither the plants nor the supports obstruct the light path during imaging. C. Side by side pictures of the ZEISS glass capillary (left) and MAGIC (right), both mounted into the metal sample holder. D Schematic showing MAGIC mounted and locked into the metal holder provided by ZEISS. Photo showing MAGIC inserted into the Lightsheet Z.1. Note that the plant holder disk is visualized through the window (blue square). Zoom of MAGIC and the plants inserted in the Z.1. imaging chamber filled with water.

specimen to remain in a vertical position, enabling the plants to follow the gravity vector. Similar to the glass capillary of the Lightsheet Z.1 (Fig. 1D), MAGIC is designed to attach to the ZEISS sample holder (Fig. 1C) and to be inserted into the microscope through the upper system cavity door. In particular, MAGIC's design consists of two features: a drive shaft and a plant-holder disk (Fig. 1A). The top of the drive shaft locks into the sample holder allowing MAGIC to be controlled by the ZEISS Lightsheet Z.1-associated software (ZEN Software), such that the device has the ability to move and rotate in all dimensions. The bottom of the drive shaft is connected to the plant-holder disk. By allowing plants to be placed in a circular configuration, the shape of the plant holder takes advantage of ZEN's rotational capability, granting MAGIC the ability to image multiple samples by spinning the disk around the central axis. The plant-holder disk is designed to hold four Fluorinated Ethylene Propylene (FEP) tubes. The positions of the holes are designed to individually cross the light sheet path when imaged, such that the loaded plants do not block each other or the laser paths (Fig. 1B). Notably, the choice of FEP tubes is based on the fact that their index of refraction (1.34) closely matches that of water (1.33) and they can be used in the Lightsheet Z.1 (Kaufmann et al., 2012). Moreover, the FEP tubes allow the shoots to grow outside of the agar, permitting gas exchange during the imaging process.

2.2. MAGIC yields in parallel long-term imaging experiments

To test MAGIC's imaging capabilities we performed 3-h time-course experiments and compared the imaging outcome with plants imaged using the ZEISS glass capillary. To assess the imaging capabilities in both systems, we used plant cell division as our indicator for root growth and development. We therefore imaged the cyclin B1 marker (*pCYCB1;1:CYCB1;1-GFP*), whose expression corresponds to the G2/M phase of the cell mitotic division.

Using the traditional loading method of the ZEISS glass capillary system, where individual plants are transferred from a nutrient-rich plate into a glass capillary, we observed that the CYCB1;1 marker consistently decayed within 3 h (Fig. 2-A1). Moreover, all the cells expressing the CYCB1;1 marker were still expressing CYCB1;1 from the first time point, suggesting that these divisions were arrested in the G2 phase and no new cell divisions occurred (Fig. 2-A2). Remarkably, using the MAGIC system, in which plants are grown and imaged inside of an FEP tube, we observed ongoing cell division throughout the experiment with little decay in the marker signal (Fig. 2-B1) as new cell divisions occurred at the end of the 3-h time frame (Fig. 2-B2). Moreover, with the multiplexed capacity of MAGIC, imaging 12 biological replicates required only 9 h of microscope usage, significantly reducing the length and the economic cost of the experiment compared to the 36 h required for the glass capillary system.

To further test MAGIC's long term imaging capacities, we extended the imaging time to 48 h ($n=4$ replicates) (Supplemental video 1). Although at the end of this time lapse we saw fewer cell divisions, all the roots still showed the CYCB1;1 marker. By showing that plants imaged with MAGIC undergo cell divisions for at least 48 h, as opposed to $\sim$3 h with the manufacturer-supplied setup, we demonstrate our chamber significantly improves the imaging conditions, increasing the imaging length by >16 fold.

Supplementary material related to this article can be found online at http://dx.doi.org/10.1016/j.ydbio.2016.05.029.

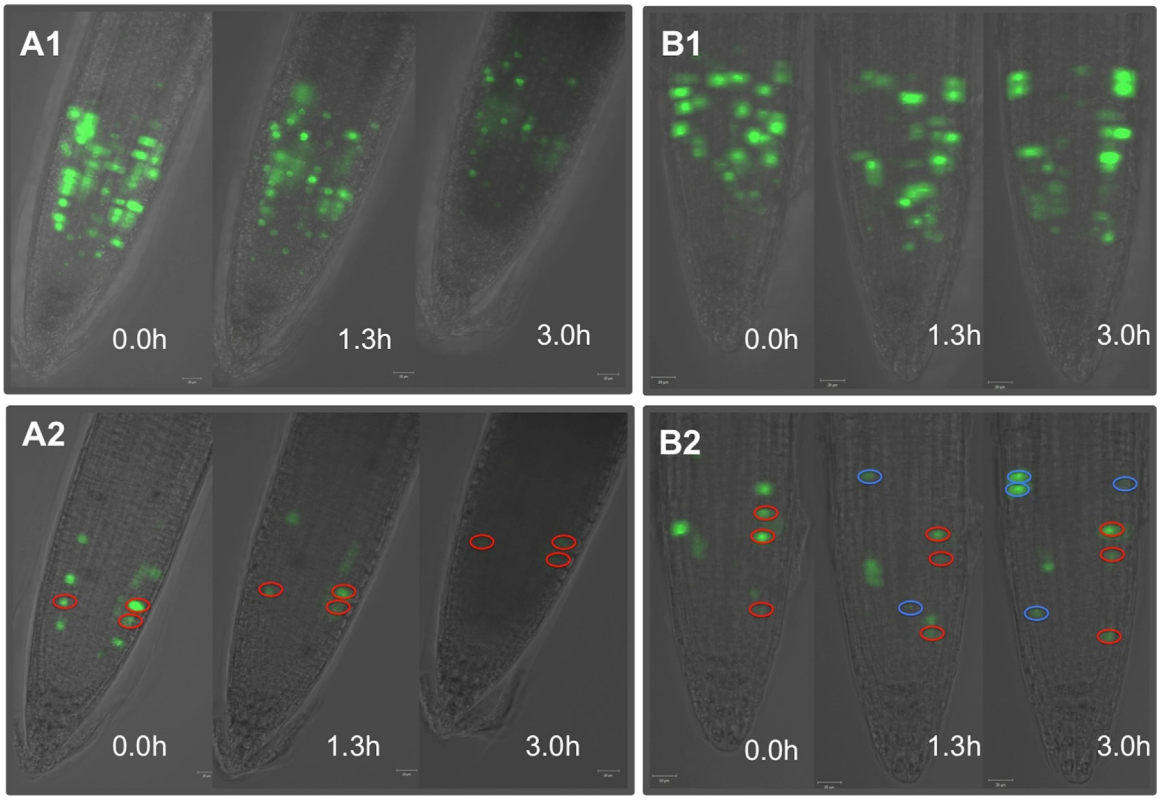

Fig. 2. Light sheet images of *pCYCB1;1:CYCB1;1-GFP Arabidopsis* roots acquired every 20 min for 3 h with the original ZEISS capillary system (A1 and 2) or MAGIC (B1 and 2). Cells expressing the *CYCB1* marker correspond to dividing cells. A1, B1. Max-projections (40 z-slices) of two selected roots. The projections show that cell divisions decrease during the time series using the capillary system (A1) while cell divisions persist throughout the time series using MAGIC (B1). A2, B2. Medial longitudinal plane of the roots shown in A1 and B1. Highlighted circles depict cells that are either not progressing (red) or progressing through the cell cycle (blue). Through the 3-h period no new divisions are visualized in the capillary system (A2), and new divisions are still observed the capillary system (B2).

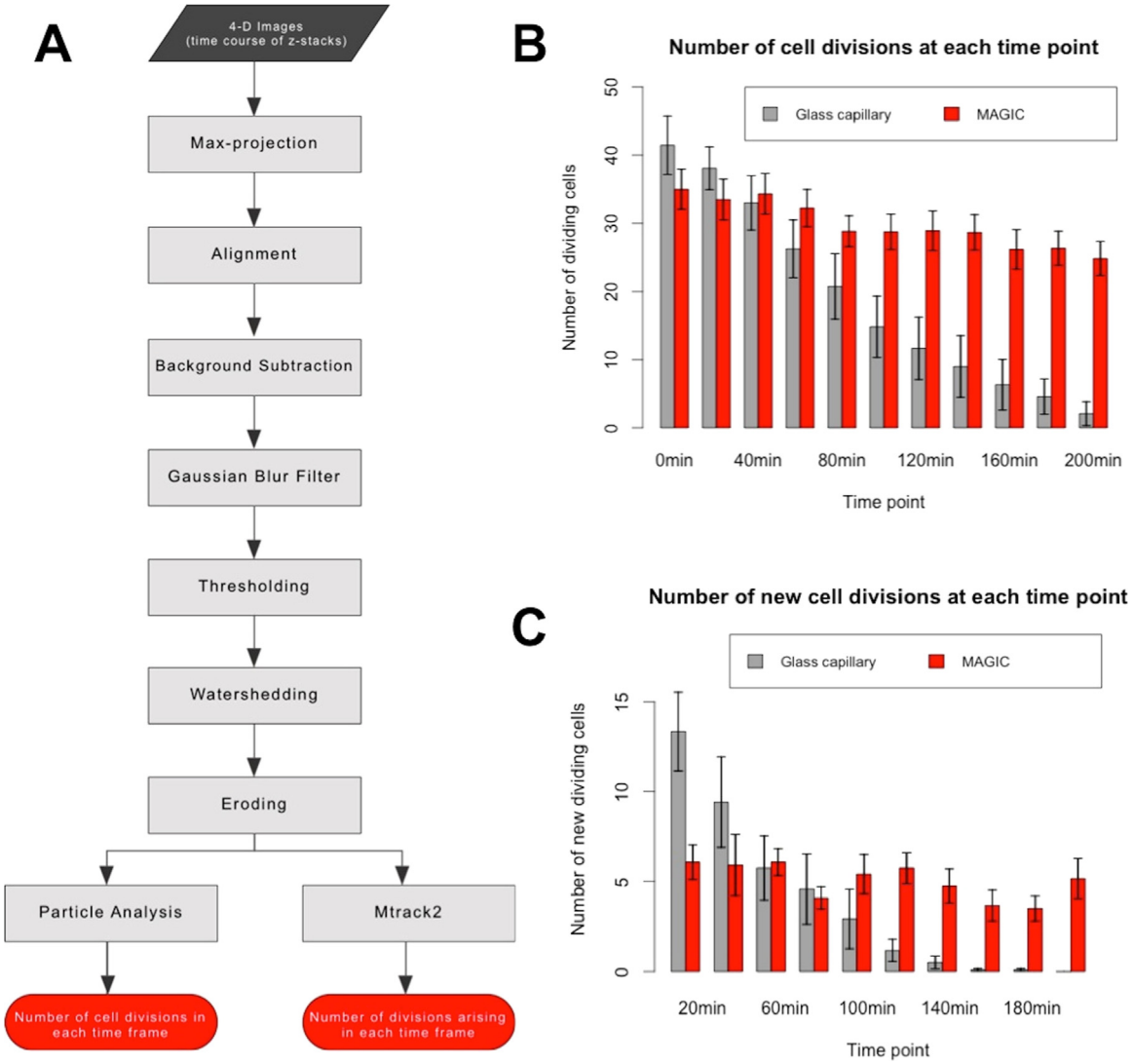

Fig. 3. A. Flow-chart of the image-processing pipeline in FIJI. B. Total number of cell divisions present at each time frame in the 3-h experiment in the glass capillary system (gray bars) and in MAGIC (red bars). C. Number of new cell divisions taking place at each time frame in the glass capillary system (gray bars) and in MAGIC (red bars). Bars represent an average of the cells quantified across biological replicates in each of the imaging systems (n = 12). Error bars represent the standard error of the mean values.

2.3. An image processing pipeline automated the quantification of cell divisions

2.3.1. FIJI image processing pipeline

To evaluate whether plants would grow throughout the imaging process, we quantified the number of cell divisions that occurred during the experiments. To this aim, we quantified the number of cell divisions per time frame as well as the new cell divisions that are taking place at each time. We automated the quantifications of cell divisions by implementing an open-source image-processing pipeline in FIJI that incorporates built-in algorithms (Fig. 3). For this, we first collapsed the z-stacks at each time point into a single plane by performing a maximum-intensity projection (max-projection). Since the roots grew during the experiment, we then aligned the max-projections of each time course to place the root in the same position across time. We subsequently applied denoising operations, such as a background subtraction followed by a Gaussian Blur filter, to even the background and consequently reduce the noise. We then generated binary images by thresholding the denoised images with thresholding algorithms. This resulted in images with black pixels in the positions of high intensity, corresponding to the positions of the cells that were dividing. A potential drawback of thresholding is that it can miss some of the high intensity signals of an image. In our case, the thresholding routines were able to identify 60–72% of the total number of dividing cells. Subsequent image processing operations, such as eroding and watershedding, separated adjacent cells and adjusted the edges of the thresholded images as needed. The format of the resulting thresholded images allowed later analysis algorithms to identify each cell as a particle, and therefore quantify both the number of cell divisions at each time frame and the new cell divisions taking place at each time.

2.3.2. Quantification of cell divisions

To automatically quantify, in each time frame, the total number of cells expressing the CYCB1;1 marker, we applied the FIJI particle analysis method to the binary images. The particle analysis method performed with a 9.6% chance of incorrectly labeling a new cell division (9.6% false positive rate). We observed that an average of 19 cell divisions are taking place at each time point in the glass capillary experiment, while an average of 30 cell divisions are observed in MAGIC's experiment (Fig. 4A). In particular, the number of cell divisions observed at the end of the glass capillary experiment decreased by 94.97% with respect to the

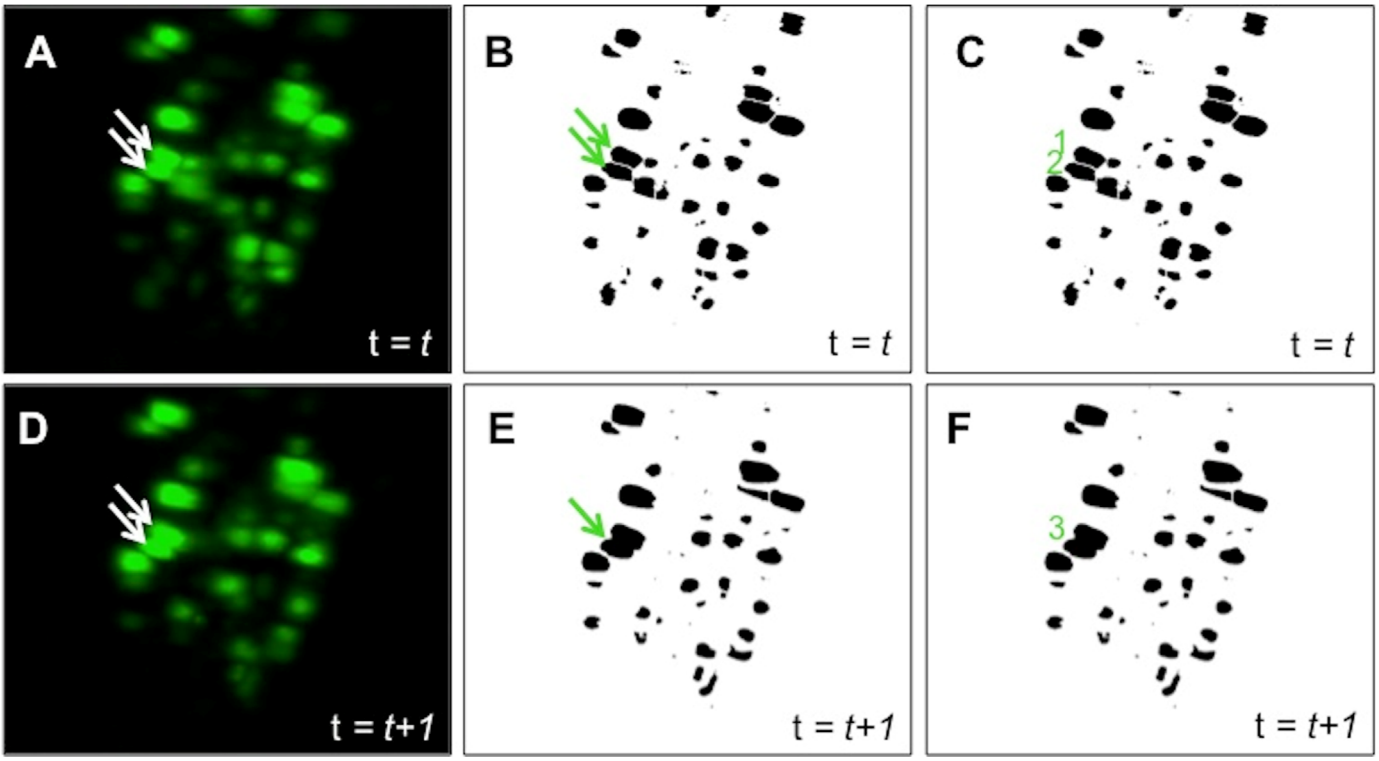

Fig. 4. Max-projection of one root of *Arabidopsis* expressing *pCYCB1;1:CYCB1;1-GFP* at two consecutive time points obtained with MAGIC. Arrows illustrate how errors in tracking cell divisions (false positive) are introduced during the image analysis. A. Max-projection of the root at time *t*. The arrows highlight two adjacent fluorescent cells. B. Max-projection from panel A after thresholding and watershedding. The arrows point to two adjacent fluorescent cells identified by the tracking pipeline as two different objects. C. Numbers represent the count of MTrack2 associated with the two fluorescent cells, 1 and 2, at time *t*. D. Max-projection of the root at time *t+1*. The arrows point to the same adjacent cells as in A. E. Max-projection from panel D after thresholding and watershedding. The arrow points to a cell that the tracking algorithm fails to separate into the two cells observed at time point *t*. F. Number associated with the count of MTrack2 at time *t+1*. Note that since the fluorescent cells are tracked through time, cells should be labeled 1 and 2. However, since these cells are not clearly separated at *t+1*, MTrack2 fails to detect that they continue to be the same objects as at time *t*. Consequently, MTrack2 labels this object as a new fluorescent cell, 3, thus leading to a false positive.

beginning of the experiment, while the decrease was only 29.06% during the imaging session performed using MAGIC.

To determine whether the CYCB1;1 expression in these experiments marked new cell divisions or cells that had become arrested in the cell cycle in the G2 phase, we applied an algorithm that could discern new cell divisions by identifying and tracking the positions of all cells expressing the CYCB1;1 marker over time. For this, we applied Mtrack2, an available FIJI plugin that automatically tracks cells. Mtrack2 allowed us to identify when new cell divisions took place with an 8.9% chance of incorrectly labeling a new cell division (8.9% false positive rate). Mtrack2 automatically determined that on average, the number of new cell divisions during the course of the glass capillary experiment decreased from 13 to 0 (100% decrease), suggesting that no new cell divisions occurred during the 3-h experiment (Fig. 4B). In contrast, the number of new cell divisions during the course of MAGIC's 3-h experiment decreased from 6 to 5 (15% decrease) indicating that cell divisions are constantly taking place (Fig. 3B).

2.3.3. *Error in the quantification of cell divisions*

Image thresholding methods operate poorly when images have inadequate contrast and show variation in gray level values within the object and its background (Chen, 2004), both of which can occur when imaging *Arabidopsis* root with the light sheet. As a result, different intensities in CYCB1 affected the thresholding operations by generating inadequate contrast or variation in gray levels, which introduced two types of error in our analysis pipeline.

First, the variation in gray levels was mainly introduced by the difference in intensities of the cells expressing the marker. This difference in intensities resulted in the thresholding routine failing to detect the dim fluorescent cells. To estimate the percentage of all the cell divisions that the FIJI-implemented thresholding methods detected, we manually counted the total number of fluorescent cells throughout each experiment. We determined that the local thresholding method was able to identify 78% of the cell divisions, while the global thresholding method could identify 60% of the cell divisions.

Second, the lack of contrast was caused by insufficient signal sharpness of the pixels surrounding brightly fluorescent cells, which complicated the distinction of the edge between two or more adjacent fluorescent cells, occasionally resulting in a single thresholded object. Consequently, the tracking plugin and particle counting algorithms led to the count of extra cell divisions (false positives) (Fig. 4). By manually counting the total number of fluorescent cells occurring in the original images, we found that an average of 9.6% of false positives was introduced by the particle analysis method, while an average of 8.9% of false positives was introduced by the tracking plugin.

3. Conclusions

We have built an imaging chamber, MAGIC, in which plants are grown and imaged in media-agar containing FEP tubes in near-physiological conditions. The designed chamber allows multiple plants to be imaged in the ZEISS Z.1 Lightsheet in a single setting, reducing previous costs and time. Despite the limitation that the plants are maintained in the dark during the imaging session, which slows down cell divisions during extended time-course

experiments, our chamber significantly improved the imaging conditions with respect to the glass capillary system. We have also presented a semi-automatic image processing pipeline that quantified cell divisions of plants imaged with both the glass capillary and our MAGIC chamber. We found that plants imaged with MAGIC underwent cell divisions >16 times longer than those imaged with the glass capillary system. These findings illustrate MAGIC's capability to further advance the use of light sheet microscopy for long time-series plant experiments. Moreover, further increasing the throughput and incorporating light emitting diode (LED) lights to generate a light-controlled environment can additionally foster MAGIC's technological potential.

4. Material and methods

4.1. MAGIC design and print

The three dimensional geometry of the chamber was designed using Solidworks (V 2014/2015 SP3), a Computer-Aided Design software. The native Solidworks file format was converted into the standard tessellation language (.stl) format using the highest resolution settings available in Solidworks. The chamber was fabricated with material jetting additive manufacturing (ASTM F2792) using an Objet Connex 350 (Stratasys inc.) PolyJet™ printer. The printer functions by selectively depositing thin layers of acrylic-based photopolymer ($\sim$16 μm thick), representing the cross sectional geometry of the component, which are cured by an ultraviolet light source immediately after deposition. The printer bed lowers the thickness of a single layer and the process repeats for the next cross section. Stratasys VeroWhitePlus™ photopolymer was used to produce the chamber. The Connex 350 printer was prepared using standard setup, cleaning and operation protocols described by the manufacturer. As is typical of polymer based additive manufacturing, all downfacing surfaces were supported by a secondary material, in this case Objet Support 705™. Parts were fabricated with the "matte" setting selected in the Connex setup software in order to ensure a homogenous surface finish. A high pressure waterjet station (Stratasys) was used to remove the supporting material from the chamber after printing and, a 1.55 mm drill bit was used to manually remove support structure from the chamber seed wells to accommodate the FEP tubing. The 3D stl models, as well as the Objet Connex 350 build file is available on the authors' website.

4.2. Plant material and growth conditions

Prior to plating, *Arabidopsis CYCB1;1:CYCB1;1-GFP* seeds (Doerner et al., 1996) were dry sterilized using 100% bleach and 1.5 mL of HCl for at least 1 h, imbibed with 500–700 μL of sterile water, and stratified for 2 days at 4 °C in complete darkness. After stratification, seeds were plated on 1 × MS (Murashige and Skooge) media supplemented with 1% sucrose and grown vertically at 22 °C in long day conditions (16 h light/8 h dark). Seedlings were grown on square plates for 5 days when imaged with the glass capillary, while seedlings were grown in 1.55 mm thick FEP tubes (Cole Parmer, EW-06406-60) for 6 days when imaged with MAGIC. Note that for plant growth in FEP tubes, 1 × MS media was filtered with a 0.2 μm syringe filter, and 1% of low-gelling agar (Sigma number A9045-25G) was then added to the filtered solution. Sterile FEP tubes were cut to 1.5 cm lengths, and 20 μL of the filtered, sterile 1 × MS 1% agar media was added to each FEP tube. The tubes were set aside for 5 min to allow for solidification. The remaining agar solution was poured into a square polystyrene plate (Genesee number 26-275) and set aside to solidify. Seeds were placed at the top of each FEP tube. Using a sterile 22-gauge syringe needle, the seeds were pushed approximately 1mm into the agar. Once the plate had solidified completely, a sterile blade was used to cut a 2 cm window in the agar (Supplementary Fig. 1). The FEP tubes containing the seeds were then vertically placed in the square hole, and the plate was sealed with parafilm and placed vertically in a Percival to grow. The FEP tubes in which seedlings were grown for 6 days were then placed into MAGIC prior to imaging (Supplementary Fig. 1).

4.3. MAGIC imaging

The microscope imaging chamber was filled with 20 mL of water, and allowed at least 20 min for temperature equilibration, set at 22 °C. The stage was pulled down such that only the roots were submerged in water; the water level in the chamber was adjusted, when necessary. The front door camera ("Locate Capillary" tab) was used to position roots 1–4, respectively, as labeled on MAGIC, and the θ-orientation was noted for each root. The acquisition interface was set up with the Plan-Apochromat 20 × / 1.0 NA water immersion detection objective lens by using the parameters specified in Supplementary Table 1.

To conduct the experiment, the z-stack, time series, multiview, and group options were activated. A z-stack of approximately 40 slices at 3.00 μm intervals was generated for each θ-orientation and was added to the multi-view option as a new "group" (G*n* corresponding to root *n*, for $n=1,2,3,4$). The z-stacks for each root were taken every 20 min for at least 12 cycles. Readjustments of the root and corresponding z-stacks were made, if necessary, as it grew out of the image frame.

4.4. Image analysis pipeline

Image analysis was performed using the FIJI software. To perform the max-projection, and since the high intensity of the initial z-planes often masked the signal of the dividing cells throughout the deeper layers of the root, 15–18% of the first planes from the z-stacks had to be eliminated. The subsequent alignment of the images through time was performed with the Linear Stack Alignment using SIFT plugin with the default parameters. The next denoising operation for subtracting the background was performed using a rolling ball of 200-pixel radius, and the Gaussian Blur filter was applied with a sigma radius of 2. Thresholding was performed with the global modified IsoData algorithm (Default method) or with the local MidGray algorithm (Parameter1 $=-5$). Although local thresholding methods are generally better suited for unevenly illuminated images, such as those from brightfield microscopy, global methods (modified IsoData) were chosen for the case in which the cell-tracking algorithm would be used, as this setting was found to introduce smaller errors in the tracking algorithm (Mtrack2). The particle analysis method was applied to the images that had been thresholded with the local thresholding method, with a size of 100-infinity pixels2 and with a circularity of 0.2–1. Mtrack2 was applied to the images that had been thresholded with the global thresholding method, with a minimum object size of 1 pixel, a maximum object size of 999999 pixels, a maximum velocity of 10, and a minimum track length of 1 frame.

Author contribution statement

M.A.L.B., M.R.P. T.J.H and R.S. designed and supervised the research. M.R.P. performed the experiments and imaging. M.A.L.B. developed the imaging pipeline and analyzed the images. M. B. R. and C.M.N.M. designed and printed the 3-D printing prototypes. E. J. supervised the imaging. M.A.L.B., M.R.P. and R.S. wrote the manuscript.

Conflict of interest

The authors declare no conflict of interest.

Acknowledgement

We thank Anna N. Stepanova, Jose M. Alonso, Robert G. Franks, Marcela Rojas-Pierce, and Cara Winter for comments on the manuscript. Support for this work was provided by the NCSU Research Innovation Seed Funding (2015-2193). Work in the Sozzani lab is also supported by the National Science Foundation (NSF) (RS: NSF CAREER MCB 1453130) and by the Bilateral BBSRC NSF/BIO (MALB: MCB 1517058).

Appendix A. Supplementary material

Supplementary data associated with this article can be found in the online version at http://dx.doi.org/10.1016/j.ydbio.2016.05.029.

References

Busch, W., et al., 2012. A microfluidic device and computational platform for high-throughput live imaging of gene expression. Nat. Methods 9, 1101–1106.
Chen, S., 2004. Chaotic spread spectrum watermarking for remote sensing images. J. Electron. Imaging 13, 220.
Doerner, P., Jørgensen, J.E., You, R., Steppuhn, J., Lamb, C., 1996. Control of root growth and development by cyclin expression. Nature 380, 520–523.
Grossmann, G., et al., 2011. The RootChip: an integrated microfluidic chip for plant science. Plant Cell Online 23, 4234–4240.
Kaufmann, A., Mickoleit, M., Weber, M., Huisken, J., 2012. Multilayer mounting enables long-term imaging of zebrafish development in a light sheet microscope. Development 139, 3242–3247.
Maizel, A., Von Wangenheim, D., Federici, F., Haseloff, J., Stelzer, E.H.K., 2011. High-resolution live imaging of plant growth in near physiological bright conditions using light sheet fluorescence microscopy. Plant J. 68, 377–385.
Novák, D., Kuchařová, A., Ovečka, M., Komis, G., Šamaj, J., 2015. Developmental nuclear localization and quantification of GFP-Tagged EB1c in Arabidopsis root using light-sheet microscopy. Front. Plant Sci. 6, 1187.
Ovečka, M., et al., 2015. Preparation of plants for developmental and cellular imaging by light-sheet microscopy. Nat. Protoc. 10, 1234–1247.
Reynaud, E.G., Krzic, U., Greger, K., Stelzer, E.H.K., 2008. Light sheet-based fluorescence microscopy: more dimensions, more photons, and less photodamage. HFSP J. 2, 266–275.
Sena, G., Frentz, Z., Birnbaum, K.D., Leibler, S., 2011. Quantitation of cellular dynamics in growing Arabidopsis roots with light sheet microscopy. PLoS One 6, 1–11.
Vermeer, J.E.M., et al., 2014. A spatial accommodation by neighboring cells is required for organ initiation in Arabidopsis. Science 343, 178–183.
Vermeer, J.E.M., Geldner, N., 2015. Lateral root initiation in *Arabidopsis thaliana*: a force awakens. F1000Prime Rep. 7, 32.
von Wangenheim, D., Daum, G., Lohmann, J.U., Stelzer, E.K., Maizel, A., 2014. Live imaging of Arabidopsis development. Methods Mol. Biol. 1062, 539–550.
Weber, M., Huisken, J., 2011. Light sheet microscopy for real-time developmental biology. Curr. Opin. Genet Dev. 21, 566–572.